



Deposited via The University of Sheffield.

White Rose Research Online URL for this paper:

<https://eprints.whiterose.ac.uk/id/eprint/169433/>

Version: Accepted Version

Article:

Maurya, S., Srivastava, P.K., Yaduvanshi, A. et al. (2021) Soil erosion in future scenario using CMIP5 models and earth observation datasets. *Journal of Hydrology*, 594. 125851. ISSN: 0022-1694

<https://doi.org/10.1016/j.jhydrol.2020.125851>

Article available under the terms of the CC-BY-NC-ND licence
(<https://creativecommons.org/licenses/by-nc-nd/4.0/>).

Reuse

This article is distributed under the terms of the Creative Commons Attribution-NonCommercial-NoDerivs (CC BY-NC-ND) licence. This licence only allows you to download this work and share it with others as long as you credit the authors, but you can't change the article in any way or use it commercially. More information and the full terms of the licence here: <https://creativecommons.org/licenses/>

Takedown

If you consider content in White Rose Research Online to be in breach of UK law, please notify us by emailing eprints@whiterose.ac.uk including the URL of the record and the reason for the withdrawal request.

1
2
3
4
5
6
7
8
9
10
11
12
13
14
15
16
17
18
19
20
21
22
23

Soil erosion in future scenario using CMIP5 models and earth observation datasets

Swati Maurya¹, Prashant K Srivastava*^{1,2}, Aradhana Yaduvanshi³, Akash Anand¹, George P. Petropoulos⁴, Lu Zhuo⁵, R K Mall²

¹Remote Sensing Laboratory, Institute of Environment and Sustainable Development, Banaras Hindu University, Varanasi-221005, India

²DST-Mahamana Centre of Excellence in Climate Change Research, Institute of Environment and Sustainable Development, Banaras Hindu University, Varanasi-221005, India

³Department of Civil Engineering, Indian Institute of Technology Bombay, Powai-400076, India

⁴Department of Geography, Harokopio University, of Athens, Athens, Greece

⁵Department of Civil and Structural Engineering, University of Sheffield, Sheffield, UK

*Correspondence: prashant.just@gmail.com; Tel.: +917571927744

Abstract:

Rainfall and land use/land cover changes are significant factors that impact the soil erosion processes. Therefore, the present study aims to investigate the impact of rainfall and land use/land cover changes in the current and future scenarios to deduce the soil erosion losses using the state-of-the-art Revised Universal Soil Loss Equation (RUSLE). In this study, we evaluated the long-term changes (period 1981-2040) in the land use/land cover and rainfall through the statistical measures and used subsequently in the soil erosion loss

24 prediction. The future land use/land cover changes are produced using the Cellular Automata
25 Markov Chain model (CA-Markov) simulation using multi-temporal Landsat datasets, while
26 long term rainfall data was obtained from the Coupled Model Intercomparison Project v5
27 (CMIP5) and Indian Meteorological Department. In total seven CMIP5 model projections
28 viz Ensemble mean, MRI-CGCM3, INMCM4, canESM2, MPI-ESM-LR, GFDL-ESM2M
29 and GFDL-CM3 of rainfall were used. The future projections (2011-2040) of soil erosion
30 losses were then made after calibrating the soil erosion model on the historic datasets. The
31 applicability of the proposed method has been tested over the Mahi River Basin (MRB), a
32 region of key environmental significance in India. The finding represents that rainfall-runoff
33 erosivity gradually decreases from 475.18 MJ mm/h/y (1981-1990) to 425.72 MJ mm/h/y
34 (1991-2000). A value of 428.53 MJ mm/h/y was obtained in 2001-2010, while a significantly
35 high values 661.47 MJ mm/h/y is reported for the 2011-2040 in the ensemble model mean
36 output of CMIP5. The combined results of rainfall and land use/land cover changes reveal
37 that the soil erosion loss occurred during 1981-1990 was 55.23 t/ha/y (1981-1990), which is
38 gradually increased to 56.78 t/ha/y in 1991-2000 and 57.35 t/ha/y in 2000-2010. The
39 projected results showed that it would increase to 71.46 t/h/y in 2011-2040. The outcome of
40 this study can be used to provide reasonable assistance in identifying suitable conservation
41 practices in the MRB.

42 **Keywords:** Soil erosion; CMIP5 model; CA-Markov; Mahi River Basin; GIS; remote
43 sensing

44

45

46 **1. Introduction**

47 Climate and land use changes are inter-related with each other. Direct effect of climate
48 change in terms of rainfall intensity, duration, magnitude (Renschler *et al.*, 1999; Pandey *et*
49 *al.*, 2007; Jain and Kumar, 2012; Rajeevan and Nayak, 2017) and indirect effect of land use
50 change in term of urban sprawl, deforestation and other human activity caused an increases in
51 the soil erosion losses. Therefore, the consequences of these climate and land use changes are
52 essential to quantify the soil erosion rate for sustainable agricultural and environmental
53 development. In India, almost 167 Mha of the area is found vulnerable to water and wind
54 erosion (Das, 2014). Food and Agriculture Organization (FAO) reported that 25 to 40 billion
55 tons of topsoil are degraded every year and it eventually impact the crop yield and soil
56 properties(Montanarella *et al.*, 2015). In general, soil erosion is a natural geological process
57 that results in the removal of soil particles by water or wind and it is transported with the
58 stream (Ganasri and Ramesh, 2016). Soil erosion is a major issue worldwide, which causes
59 losses of soil nutrients, increasing sedimentation in rivers, degradation of agricultural land,
60 high runoff and so forth. Therefore, it is imperative that natural resources should be managed
61 on a sustainable basis to ensure long-term productivity and food security (Renschler *et al.*,
62 1999; Pandey *et al.*, 2007; Gajbhiye *et al.*, 2014). Earth Observation (EO) provides detailed
63 information about land, topography, watersheds characteristics, including soil types, land use
64 and land cover and geomorphology. This information can also be easily integrated with
65 Geographical Information Systems (GIS) to provide a quantitative measure of soil erosion.

67 Various models developed in the past for soil losses assessment such as Water Erosion
68 Prediction Project (WEPP), Soil and Water Assessment Tool (SWAT), Universal Soil Loss
69 Equation (USLE), Revised Universal Soil Loss Equation (RUSLE) and others. Among all
70 updated version of USLE i.e. RUSLE model is widely used and worldwide accepted due to
71 its ability to provide an accurate estimation of soil erosion both quantitatively and spatially
72 (Renard *et al.*, 1991; Kouli *et al.*, 2009; Bonilla *et al.*, 2010; Nagaraju *et al.*, 2011a;
73 Prasannakumar *et al.*, 2012; Tirkey *et al.*, 2013; Karamesouti *et al.*, 2016). A lot of studies
74 conducted over the Indian region such as Thomas *et al.*(2018) reported a severe rate of soil
75 loss in the tropical mountain river basin of Western Ghats, India using RUSLE with the
76 transport limited sediment delivery (TLSD) function (Thomas *et al.*, 2018). Kumar *et*
77 *al.*(2014) suggested that soil erosion in the Himalayan watershed is a very sensitive factor
78 as high slope and depleting forest covers are major causes of erosion (Kumar *et al.*, 2014).
79 In the last few decades, with the advancements in satellite observations and data quality,
80 there is a substantial increase in the research studies on the impact of land use and rainfall
81 on soil erosion. (Markose and Jayappa, 2016) used the RUSLE model in a tropical humid
82 climatic zone that is experiencing a severe loss in soil due to natural factors, whereas,
83 (Wang *et al.*, 2018) compared the effects of rainfall and land use land cover patterns on soil
84 erosion for different watersheds which is likely to play a crucial role in modelling and
85 management of multi-scale watersheds. Another study by (Wei *et al.*, 2007) considered the
86 influence of different rainfall patterns to estimate the impact of land use on the soil erosion,
87 and concluded that the concentration as well as high intensity with short duration rainfall
88 events influences the soil erosion processes.

89 Additionally, Global Climate Models (GCMs) have been successfully used in the scientific
90 community for future climate projections. In general, their resolution is not enough to
91 produce the regional climatic condition. Therefore in this study the NEX-GDDP (NASA
92 Earth Exchange Global Daily Downscaled Projections) based Coupled Model
93 Intercomparison Project Phase (CMIP5) data at fine resolution $0.25^0 \times 0.25^0$ (Bao and Wen,
94 2017) is employed. In the purview of the above, the focus of this study is to assess the impact
95 of both climate and land use/land cover changes on soil erosion using the RUSLE model. In
96 order to achieve the objectives, we investigated the NEX-GDDP-CMIP5 model performance
97 over the study area for rainfall and estimated the land use/land cover changes using the
98 multirate Landsat satellite images. Future projections of landscape changes are also
99 estimated through CA-Markov and by using the classified multirate satellite images of the
100 historical time period. Afterwards, soil erosion losses were provided for the baseline and
101 future scenarios.

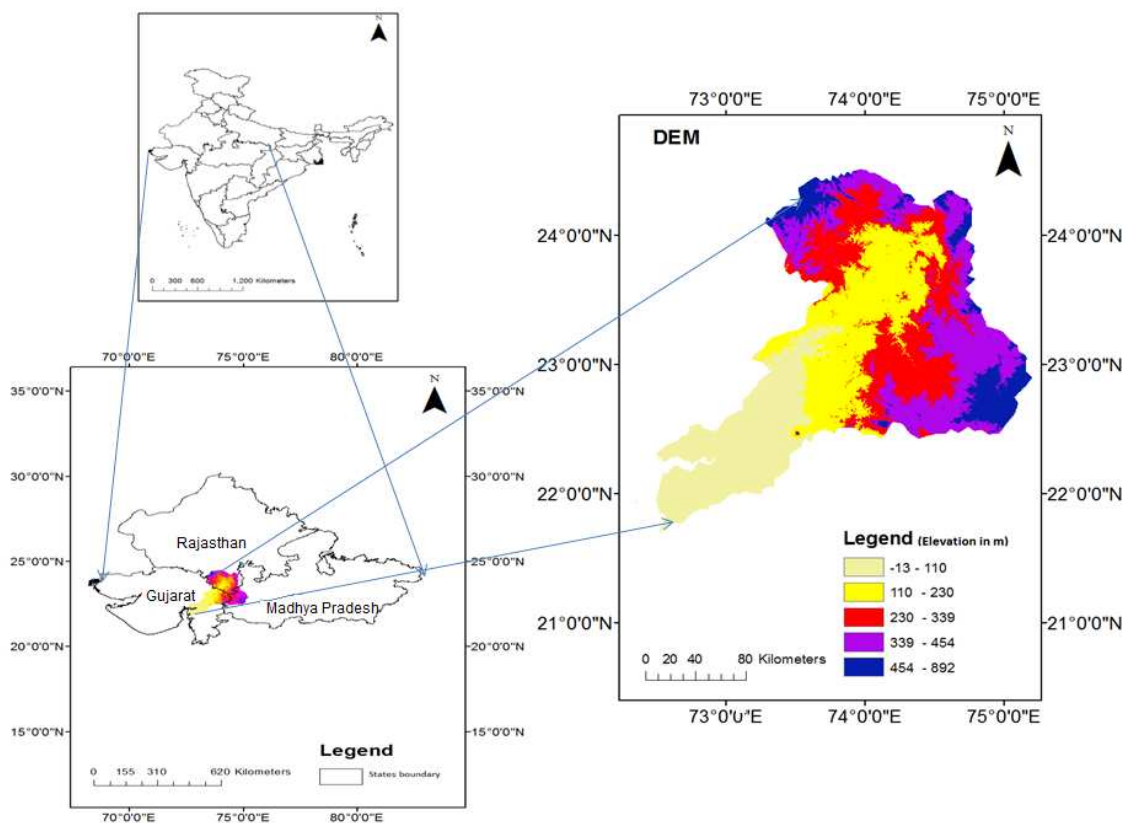
102

103 **2. Study area**

104 Mahi River is one of the largest rivers in India passing through the three geographically
105 larger states Madhya Pradesh, Rajasthan and Gujarat and terminated at the Gulf of Khambhat
106 as shown in **Figure 1**. The MRB covers an area of $34,842 \text{ km}^2$. The basin can be divided into
107 three parts-lower, middle and upper part. The upper part of the basin is having mostly hills
108 and forests with some plain area in Madhya Pradesh. The middle part is having developed
109 lands and mostly found in Gujarat. The Gujarat region is also encompassing most of the
110 lower basin, which is very fertile with alluvial soil. In MRB, the area that can be used for

111 agriculture is around 2.21 Mha. The other soil types which are found in the basin are red and
112 black soils. Hydro-geologically the basin is dominated by basaltic rocks with trappean. The
113 average rainfall in MRB is approx. 785 mm. Apart from agriculture, it is one of the important
114 sources for irrigation, drinking water and industrial water demand.

115



116

117 **Fig.1. Location map of Mahi River Basin, India.**

118

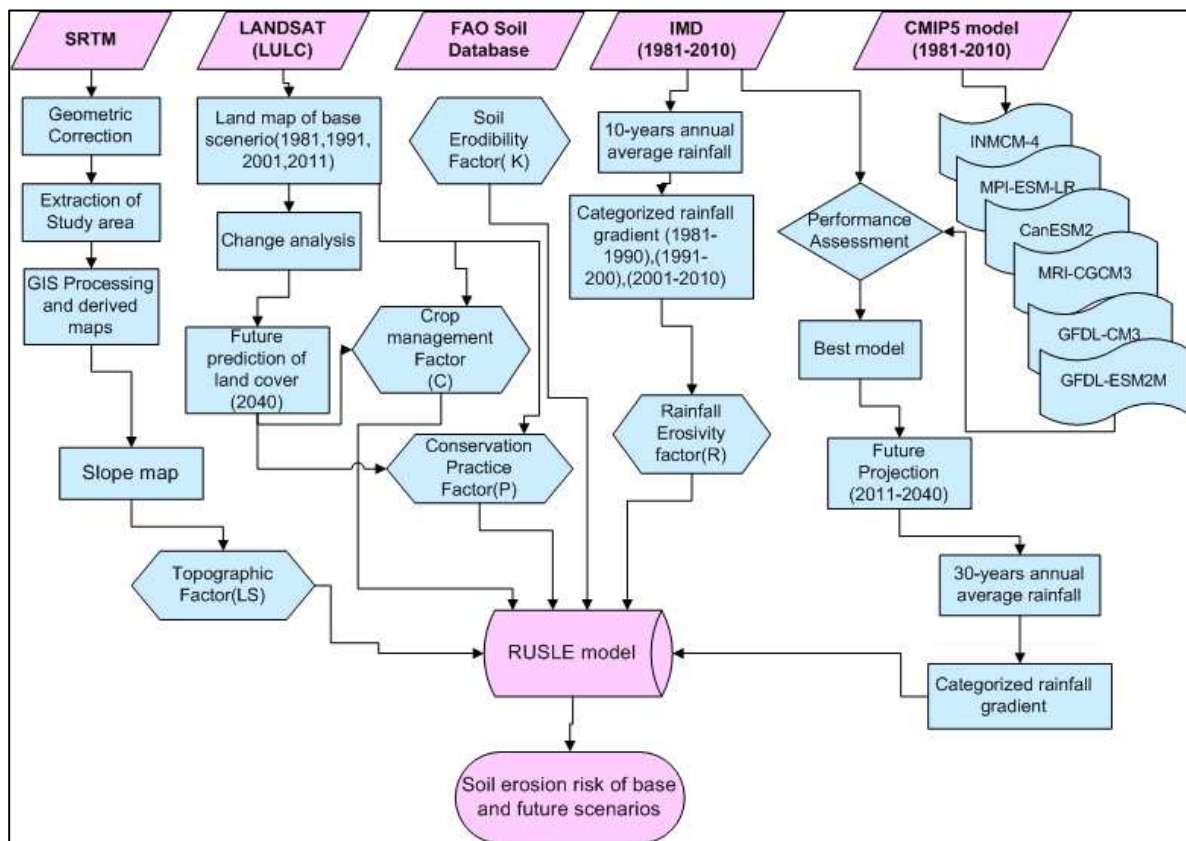
119 **3. Materials and Methods**

120 In this study, the NASA-NEX-GDDP-CMIP5 model output, IMD (observed) datasets, Land
121 use/land cover from Landsat were used. Along with the assessment, the future land cover
122 expansion and climate change scenarios are also considered for their potential impacts on soil

123 erosion in MRB. To achieve this objective, an integrated approach of an erosion model,
 124 climate model and land use/land cover datasets has been used. The methodology of the
 125 present study has been summarized in **Figure 2**. The detailed description of datasets and
 126 methodology are provided in sub sections.

127 3.1 Digital Elevation Model (DEM)

128 The Shuttle Radar Topography Mission (SRTM) launched in collaboration between
 129 NASA and the National Geospatial Intelligence Agency (NGA). It provides void filled
 130 elevation data globally (<http://www.cgiarcsi.org>). In the present study, a 30 m DEM (v.3) is
 131 used for the extraction of slope of the study area using the spatial analyst tool of Arc GIS 10.1
 132 software (**in Figure 3(a)**). Slope expressed the inclination of landform associated with the
 133 physical feature. Higher slope value leads to rapid runoff with potential soil erosion
 134 (Stefanidis and Stathis, 2018).



135

136

137

Fig.2. Workflow of the methodology developed in this study

138

139 **3.2 IMD Rainfall datasets**

140 The Indian Meteorological Department (IMD) provided the gridded daily rainfall data at

141 $0.25^0 \times 0.25^0$. The daily rainfall recorded from 6955 rain gauge stations of National Data

142 Centre, IMD, Pune, India (Pai *et al.*, 2014). IMD uses the Inverse Distance Weighted

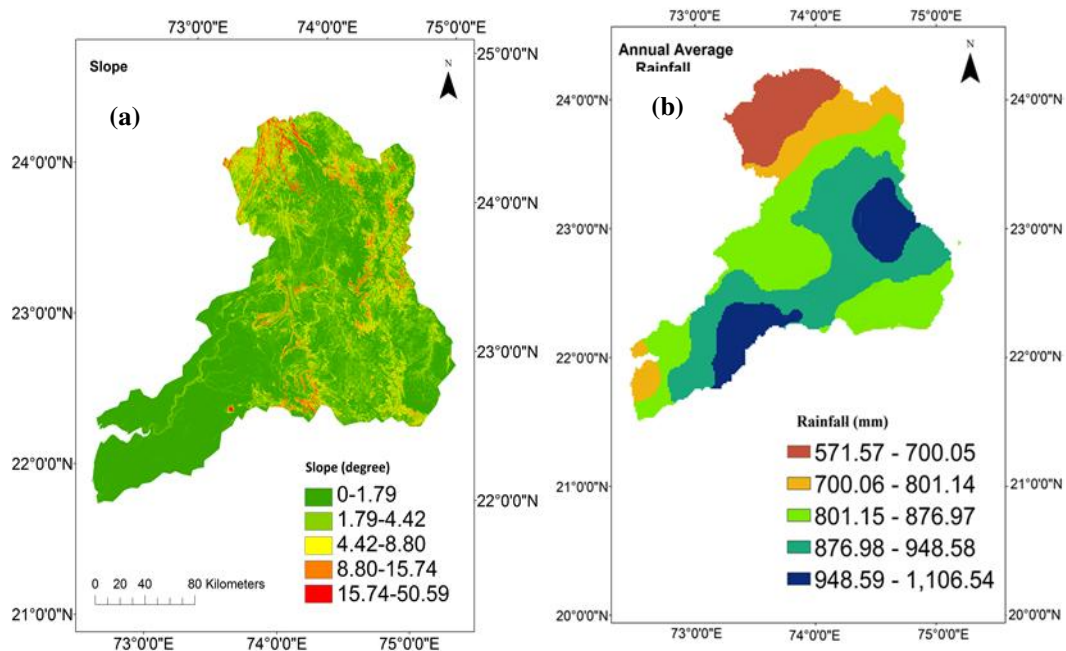
143 interpolation technique along with the radial distance to convert the point-based gauge data

144 into grid data. 30 years (1981-2010) of annual average rainfall data have been used,

145 obtained for the meteorological stations Dhariawad, Mataji, Rangeli, Chakaliya, Paderibadi,

146 Khanpur in the study area (**Figure 3(b)**) .

147



148

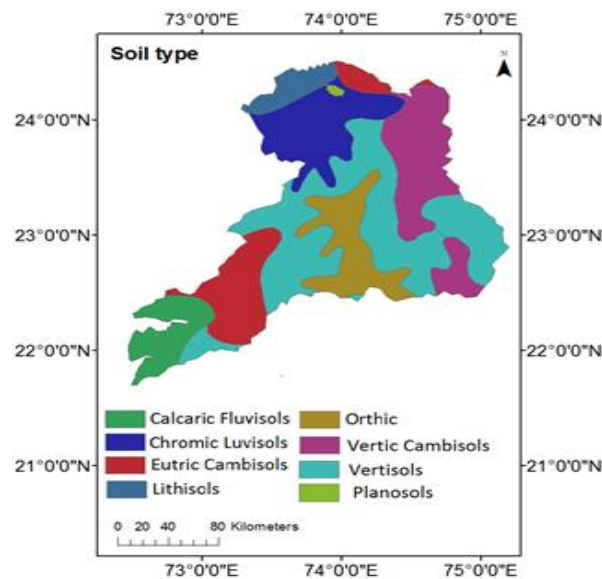
149

150 **Fig.3. (a) Slope map (b) Annual average rainfall (1981-2010)**

151

152 **3.3 Soil map**

153 Soil map data is obtained from the FAO, United Nations, at 1:5000,000 scale and
154 the dataset can be obtained at no cost from
155 FAO([http://www.fao.org/soils-portal/soil-survey/soil-maps-and-databases/faounesco-soil-m
157 ap-of-the-world](http://www.fao.org/soils-portal/soil-survey/soil-maps-and-databases/faounesco-soil-m
156 ap-of-the-world)). It provide information related to soil properties at the depth 0 – 30 cm
158 (topsoil) and 30 – 100 cm (subsoil) with various parameters as Organic Carbon, pH(H₂O),
159 Calcium carbonate, Sand fraction, Silt fraction, Clay fraction, Bulk Density and so on. The
160 data showed that the study region is mainly covered by eight soil classes as shown in**Figure**



161

162

163

Fig. 4. Soil map of the area

164

165

166

167 **3.4 Land use/land cover estimation and prediction**

168 Landsat satellite data is used for land use/land cover estimation. Landsat is a collaborative
169 effort of the US Geological Survey and the National Aeronautics and Space Administration
170 (NASA). In this study, Landsat 1-5 having MSS (Multispectral scanner) and TM (Thematic
171 Mapper) sensors data are used to prepare land use/land cover maps for the years 1981, 1991,
172 2001, 2011. Before the classification of the images, they are geo-referenced and projected to
173 WGS 1984 UTM Zone 43N coordinate system. In ENVI software, Support Vector Machine
174 (SVM) algorithm based supervised classification system is applied to classify the images.
175 SVM is found to be the best algorithm for land use/land cover classification by many
176 researchers (Srivastava *et al.*, 2012; Singh *et al.*, 2014; Nandi *et al.*, 2017; Fragou *et al.*,
177 2020). The study area is classified into five classes namely, Waterbody, Cropland, Grassland,
178 Barren, Urban and Forest land respectively. **Table 1** is showing the overall classification
179 accuracy and the Kappa performance statistics, which is 78.3%, 82.7%, 80.8%, 88.4% and
180 0.76, 0.79, 0.77, 0.85 respectively for the classified images of the year 1981, 1991, 2001 and
181 2011. Further, the state of the arts CA-Markov has been used for the prediction of land
182 use/land cover classes of 2040 as shown in **Figure 5**. CA-Markov model is one of the most
183 commonly used and consistent model for simulating land use/land cover changes, it
184 combines cellular automata and Markov chain to predict the changes through space and time
185 (Weng, 2002). CA-Markov is widely used in several studies such as in ecological
186 modelling (Ghosh *et al.*, 2017), watershed management (Yulianto *et al.*, 2018), urban growth
187 (Aburas *et al.*, 2017) and land use policy designing (Liu *et al.*, 2017). Mathematical
188 expression for the CA-Markov model can be understood through Eq. 1 and 2

189 $S(t, t + 1) = P_{ij} * S(t)$ (1)

190
$$\|P_{ij}\| = \begin{vmatrix} P_{1,1} & P_{1,2} & \dots & P_{1,n} \\ P_{2,1} & P_{2,2} & \dots & P_{1,n} \\ \dots & \dots & \dots & \dots \\ P_{n,1} & P_{n,1} & \dots & P_{n,n} \end{vmatrix}$$
 (2)

191 Where S(t) is the image at time t, S(t+1) is the image at time t+1 and P_{ij} is the transition
 192 probability matrix in which i is the current state and j is the future state. The value of P_{ij}
 193 varies from 0 to 1 in which the low transition probability will be near to 0 and high transition
 194 probability will be near to 1.

195 **Table. 1 Accuracy assessment of land use/land cover classification**

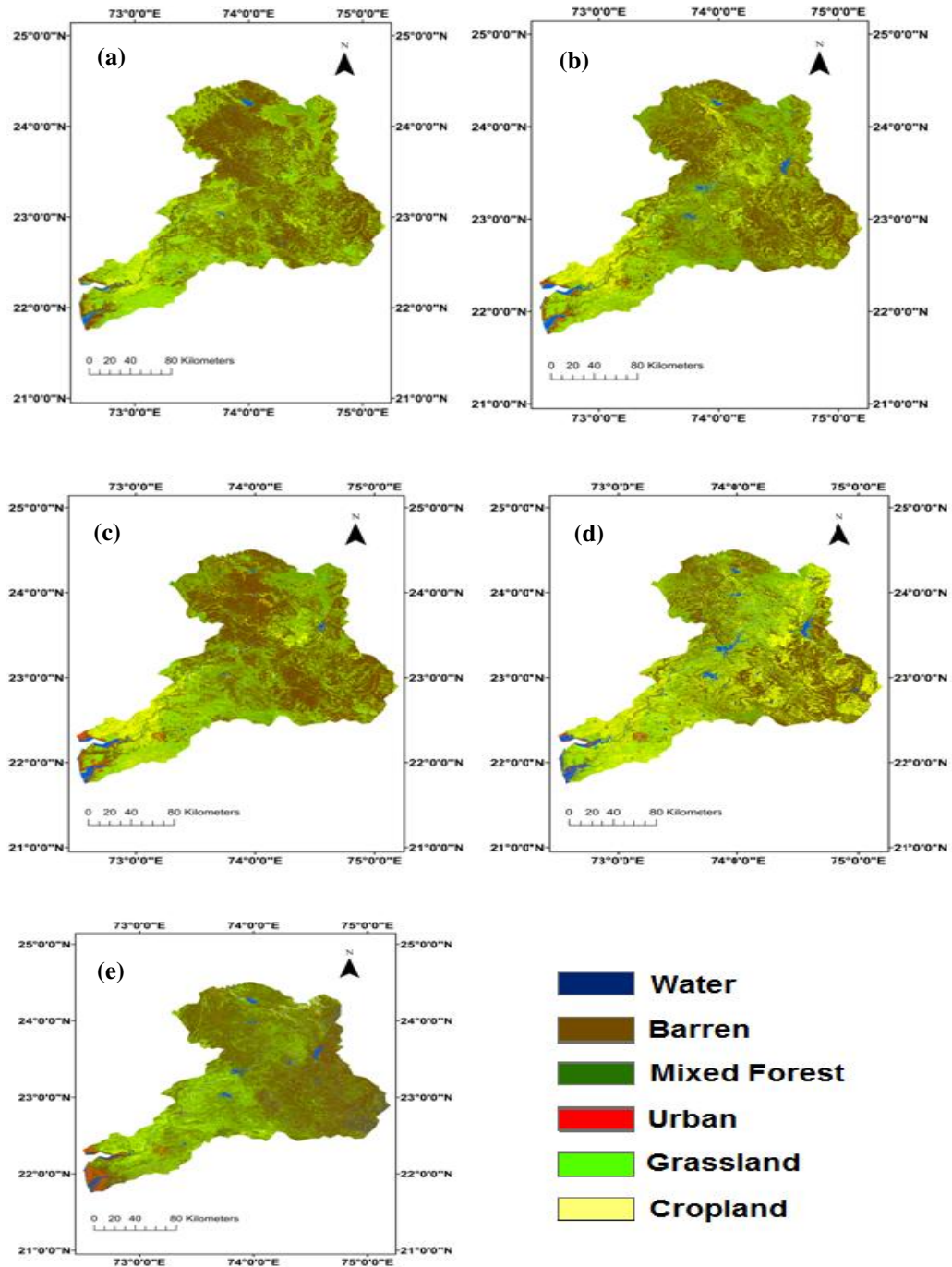
196

<i>Land Use/Land Cover Classes</i>	<i>1981</i>		<i>1991</i>		<i>2001</i>		<i>2011</i>	
	<i>PA(%)</i>	<i>UA(%)</i>	<i>PA(%)</i>	<i>UA(%)</i>	<i>PA(%)</i>	<i>UA(%)</i>	<i>PA(%)</i>	<i>UA(%)</i>
<i>Waterbody</i>	100	98.8	96.6	100	100	96.2	100	98.5
<i>Forest</i>	82.4	78.6	92.0	88.2	87.5	93.6	94.2	91.7
<i>Grassland</i>	84.5	78.3	88.0	84.5	76.2	72.5	87.2	88.5
<i>Cropland</i>	70.3	78.5	83.3	80.0	77.2	81.0	82.5	84.1
<i>Barren</i>	88.0	84.5	78.2	75.5	85.6	88.2	79.6	75.5
<i>Urban</i>	67.2	69.2	75.5	79.4	68.4	71.2	84.2	87.1
<i>Overall Accuracy</i>	78.3		82.7		80.8		88.4	

<i>Kappa Accuracy</i>	0.76	0.79	0.77	0.85
-----------------------	------	------	------	------

197 *Producer Accuracy (PA), User Accuracy (UA)

198



199

200 **Fig.5 Spatial distribution of land use/land cover (a) 1981, (b) 1991, (c) 2001,**

201 **(d) 2011, and (e) 2040.**

202

203 **3.5 Global Climate Model data**

204

205 The NEX-GDDP datasets are downscaled climate scenarios derived from the General
206 Circulation Model (GCM) simulations of the Coupled Model Intercomparison Project Phase
207 5 (CMIP5). The four major greenhouse gas emissions scenarios are considered as
208 Representative Concentration Pathways (RCPs) based on IPCC AR5 (Intergovernmental
209 Panel on Climate Change–Fifth report). The NEX-GDDP dataset uses statistical downscaling
210 approach namely-Bias-Corrected Spatial Disaggregation (BCSD) method to downscale the
211 projections for RCP 4.5 and RCP 8.5 from the 21 CMIP5 models (Wood *et al.*, 2004; Maurer
212 and Hidalgo, 2008). Detail document is available at <https://cds.nccs.nasa.gov>. Daily scale
213 data for maximum temperature, minimum temperature and precipitation at fine resolution
214 0.25° (~25km×25km) are available at <https://cds.nccs.nasa.gov/nex-gddp/>. In this study,
215 seven GCMs of CMIP5 were selected, which work well over the Indian region and have been
216 validated by (Bokhari *et al.*, 2018; Jain *et al.*, 2019; Sahany *et al.*, 2019). The institution,
217 country and spatial resolution of the seven models are shown in **Table 2**. The long term
218 rainfall datasets from (1981-2040) were obtained for all the seven models using the
219 NEX-GDDP-CMIP5.

220 **3.6 Evaluation of the CMIP5 Model output**

221 The performances of seven models of NEX-GDDP-CMIP5 (six model output and one
222 ensemble) were assessed by both statistical measures and spatial patterns of mean annual
223 precipitation. Taylor diagram (Taylor, 2001) is a suitable tool for the assessment of the model

224 performance through the statistical measures in terms of spatial correlation coefficient,
 225 centred pattern Root Mean Square (RMS), and the ratio of spatial standard deviations. Taylor
 226 diagram is user-friendly because of three metrics at a single platform. The circle centred at
 227 the observed point represents the RMS and the circle centred at the origin point represents the
 228 standard deviation and the correlation coefficient. For the best performance in terms of the
 229 spatial correlation and standard deviation, the value should be close to 1 and for RMS the
 230 value should be close to 0.

231 **Table. 2 Features of the six CMIP5 global climate models.**

CMIP5 Models	Institution, Country	Atmospheric Resolution	NEX-GDDP resolution
1-Geophysical Fluid Dynamics Laboratory Climate Model, version3 (GFDL-CM3)	National Oceanic and Atmospheric Administration, Geophysical Fluid Dynamics Laboratory, U.S.A	2.5° X 2°	0.25°X 0.25°
2-Institute of Numerical Mathematics Coupled Model, version 4.0	Institute of Numerical Mathematics, Russia	2°X1.5°	0.25°X 0.25°

(INMCM-4)			
3-Max Plank Institute Earth System Model, low resolution (MPI-ESM-LR)	Max Plank Institute for Meteorology, Germany	1.875°X1.8653°	0.25°X 0.25°
4-Meteorological Research Institute Coupled Atmosphere–Ocean General Circulation Model, version 3 (MRI-CGCM3)	Atmosphere and Ocean Research Institute (The University of Tokyo), National Institute for Environmental Studies, Japan	1.125°X1.1215°	0.25°X 0.25°
5-The second–generation Canadian Earth System model (CanESM2)	Canadian Centre for Climate Modelling and Analysis, Canada	2.8125°X2.7906°	0.25°X 0.25°
6-Geophysical Fluid Dynamics Laboratory Earth System Model with Modular Ocean Model,	National Oceanic and Atmospheric Administration, Geophysical Fluid	2.5°X 2.0225°	0.25°X 0.25°

version 4 (GFDL-ESM2M)	Dynamics Laboratory, U.S. A		
-------------------------------	------------------------------------	--	--

232

233 **4. Revised Universal Soil Loss Equation (RUSLE) model**

234 RUSLE was invented by the USDA-Agricultural Research Service for the conservation
235 planning and management. Originally USLE (Wischmeier and Smith, 1978) was developed
236 to predict soil loss by unit plot condition in tropics region based on rainfall, soil type,
237 topography, crop pattern and management practices. The revised version i.e. RUSLE was
238 later proposed with some modifications in the algorithm of USLE factors (Moore and
239 Wilson, 1992; Renard *et al.*, 1997). RUSLE is a spatially distributed model and does not
240 required too much data for the computation as well as it provide valuable results verified by
241 various research articles. (Fernandez *et al.*, 2003; Yue-Qing *et al.*, 2008; Demirci and
242 Karaburun, 2012; Naqvi *et al.*, 2013; Pan and Wen, 2014; Pradeep *et al.*, 2015). It provide
243 the annual average soil loss in (t/ha/y) by the following equation (Renard, 1997):

244
$$A = R \times K \times LS \times C \times P \qquad (3)$$

245

246 Where A= Average Soil Loss Per Unit Area (t/ha/y); R= Rainfall-Runoff Erosivity Factor
247 (MJ mm ha⁻¹h⁻¹year⁻¹); K = Soil Erodibility Factor (metric tons ha⁻¹MJ⁻¹mm⁻¹); LS =
248 Topographic Factor (dimensionless); C = Cover Management Factor (dimensionless); and P
249 = Conservation Practice Factor (dimensionless). Detailed descriptions of each of the RUSLE
250 component are covered in the following subsections.

251

252 **4.1 Soil Erodibility Factor (K)**

253 The K factor represents the susceptibility of soil detachment, or transportation of soil
254 particles due to rainfall. K factor significantly affected by soil structure, texture, organic
255 content, and hydraulic properties of soil. The K values (tons/ha/MJ) can be calculated by the
256 following equation (Sharpley and Williams, 1990).

257
$$K = A \times B \times C \times D \times 0.1317 \quad (4)$$

258 where:

259
$$A = [0.2 + 0.3 \exp(-0.0256SAN(1 - SIL/100))] \quad (5)$$

260
$$B = \left[\frac{SIL}{CLA + SIL} \right]^{0.3} \quad (6)$$

261
$$C = \left[1.0 - \frac{0.25C}{C + \exp[(3.72 - 2.95)]} \right] \quad (7)$$

262
$$D = 1.0 - \frac{0.70SN1}{SN1 + \exp[(-5.41 + 22.9SN1)]} \quad (8)$$

263

264 Where; SAN, SIL and CLA represents the percentage of sand, silt and clay, respectively; C
265 = organic carbon content; SN1 = sand content subtracted from 1, divided by 100.

266 Soil maps are the basic layer for the estimation of the K factor. Firstly, the vector layer of the
267 soil map is converted into raster format by ArcGIS 10.1 software. After which, k values are
268 assigned to the map by using reclassify tool of the ArcGIS 10.1.

269

270 **4.2 Rainfall-runoff Erosivity (R) factor**

271 R represents how the rainfall frequency, intensity, duration of rainfall and rate of runoff
272 affects the soil erosion. Originally, R factor estimated by the long term average of rainfall

273 kinetic energy and the maximum 30 min intensity during the storm event(Arnoldous, 1980).

274 Due to the scarcity of the data, here we used the equation based on the annual average rainfall

275 datasets (Wischmeier and Smith, 1978).

$$276 \quad R = 38.5 + 0.35r \quad (9)$$

277 Where; R = Rainfall Erosivity Factor (MJ mm ha/ h /year); r = Annual Average Rainfall

278 (mm).

279

280

281 **4.3 Conservation Practice Factor (P)**

282 The P factor represent the support practices that are applied in the field to reduce the rate of

283 runoff, to control the flow and velocity of runoff, to change the pattern of runoff and so forth.

284 P is the ratio of soil loss with a specific support practice to the corresponding slope tillage

285 (Wischmeier and Smith, 1978; Renard *et al.*, 1997). P factor values varies from 0 – 1 (Renard

286 *et al.*, 1997). P of 1 assign to those areas where have poor conservation practices (i.e., scrub

287 land, wasteland, Urban) while 0 or 0.3 value assigned to those areas where have good

288 conservation practices .

289

290 **4.4 Topographic Factor (LS)**

291 Slope length (L) and slope steepness (S) are jointly expressed as LS. L is defined as the

292 distance of flow path from the origin of overland flow to the point where deposition begins or

293 runoff water enters in a flow channel, and S is the steepness of slope (Pradhan *et al.*, 2012).

294 LS can be evaluated by field measurement or using DEM via the following equation:

295 $LS = (\text{flow accumulation} \times \text{cell size}/22.13)^{0.4} \times \sin(\text{Slope}/0.896)^{1.3}$ (10)

296 Where flow accumulation represents the number of grid cells that shows the flow downward;
 297 cell size is the grid cell size (30m is used in this study); sin Slope is the slope degree in sin.

298

299 **4.5 Crop Management Factor (C)**

300 C-factor is the most important factor after the topography. It shows the cropping pattern,
 301 management practices and the erosion control measure of soil loss (Mati *et al.*, 2000). The
 302 C-factor is decided based on land use/land cover classes as shown in **Table 3**.

303

304 **Table.3 C-Factor of the Mahi River Basin taken from the different studies**

Land Use/Land Cover	C-factor	References	305
Mixed forest	0.003	(Ganasri and Ramesh, 2016)	306
Shrubland	0.18	(Rao, 1981b)	307
Grassland	0.05	(Rao, 1981b)	308
Cropland	0.28	(Rao, 1981b)	309
Urban	1.0	(Tirkey <i>et al.</i> , 2013)	310
Barren or Sparsely vegetated	0.33	(Rao, 1981b)	311
Water	0.00	(Ganasri and Ramesh, 2016)	312

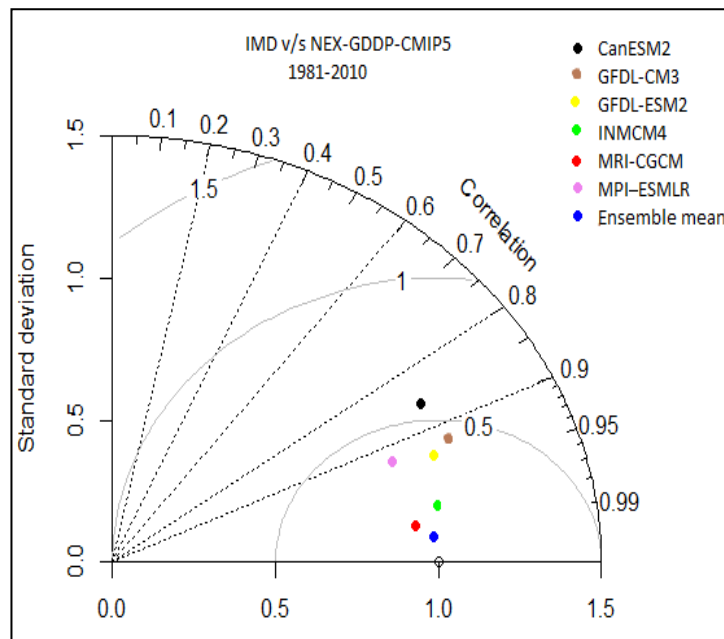
313 **ion**

314 **6.1 Performance assessment NEX-GDDP-CMIP5 outputs**

315 Taylor diagram presents a comparison of IMD data (i.e., the station observations) with the
 316 NEX-GDDP-CMIP5's six models output data and ensemble for the period 1981-2010

6.
Results
and
Discuss

317 **Figure 6.** Taylor diagram shows that all individual model and ensemble mean cluster lies in
 318 between a correlation coefficient of 0.5 to 0.85. However, standard deviation value of
 319 MRI-CGCM3, INMCM4 and Ensemble mean is close to 0.75 mm/day with an RMS value
 320 approx. 0.075 mm/day. The INMCM4 and MRI-CGCM3 showed a slightly higher RMS
 321 (0.18 and 0.13mm/day) than Ensemble model. Moreover, ensemble value reduces the
 322 uncertainty (i.e., parametric, structural and response) of individual model and showed a good
 323 performance (Giorgi and Mearns, 2002; Hagedorn *et al.*, 2005; Palmer *et al.*, 2005;
 324 Chaturvedi *et al.*, 2012). The monthly mean rainfall of the individual models and ensemble
 325 mean climatology over the MRB is shown in **Figure 7**. These plots illustrate that the
 326 MRI-CGCM3 and INMCM4 along with the ensemble mean are all underestimated but show
 327 similar pattern to the IMD, while the other models (i.e., canESM2, MPI-ESM-LR,
 328 GFDL-ESM2M and GFDL-CM3) indicated a large inter-model difference.



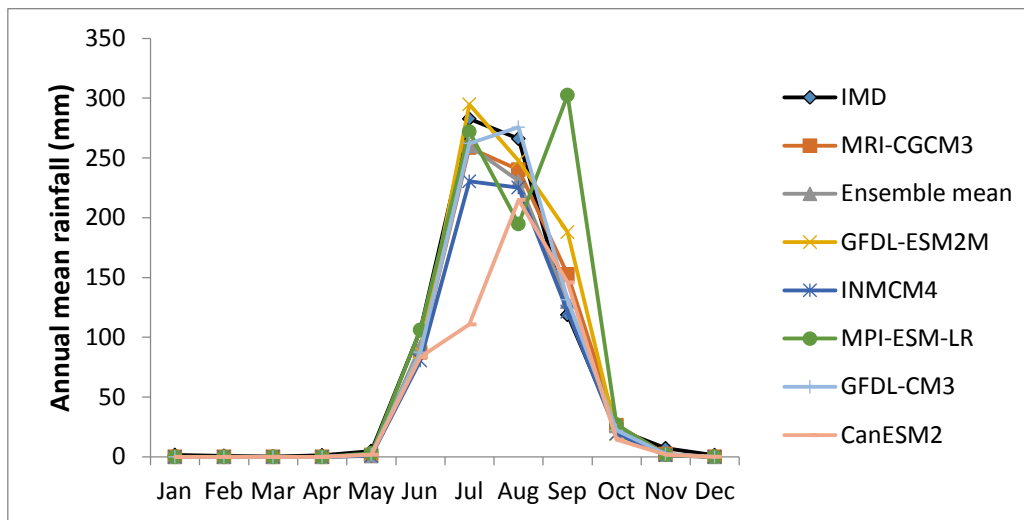
329

330

331 **Fig. 6 Performances of NEX-GDDP-CMIP5 model outputs during the monsoon**
 332 **months (1981-2010)**

333

334



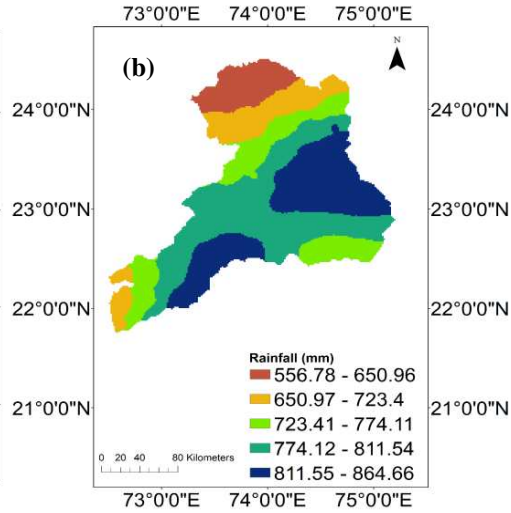
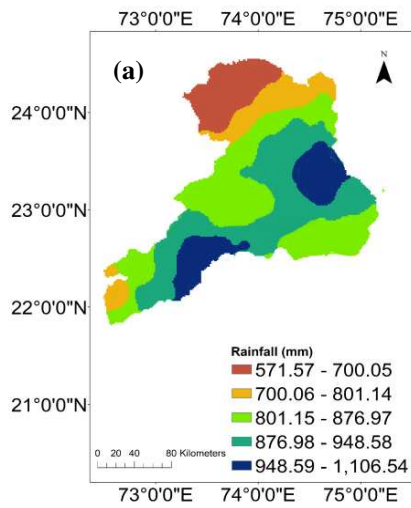
335

336 **Fig. 7 Annual mean rainfall of the IMD, NEX-GDDP-CMIP5 models and the**
 337 **Ensemble mean during the period 1981-2010**

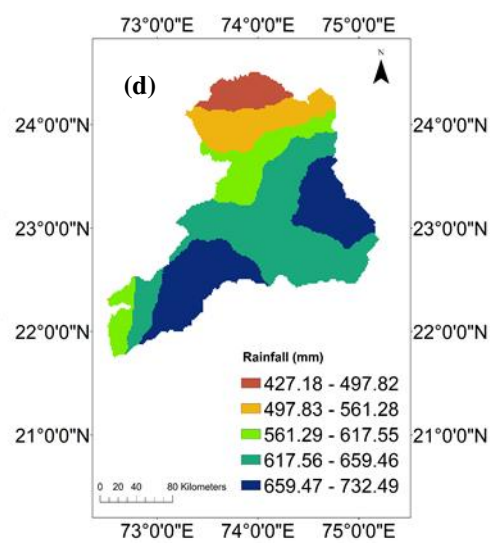
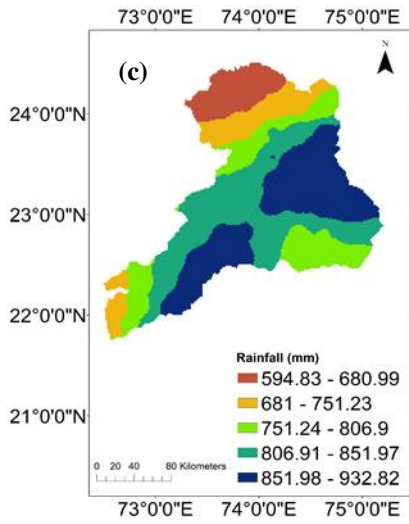
338

339 Furthermore, the spatial variabilities of the annual mean rainfall for the IMD and the
 340 NEX-GDDP-CMIP5 models are shown in **figure 8 (a-h)**. IMD has the highest rainfall
 341 gradient occurred in the north-east and the north-west parts, with moderate to low rainfall
 342 that is occurred in the north-west part of the MRB. A similar spatial distribution observed in
 343 the best performing models i.e., MRI-CGCM3, INMCM4 and ensemble mean in comparison
 344 to other models.

345



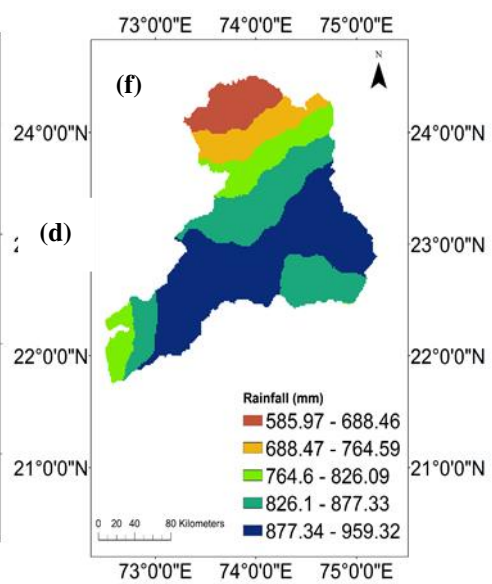
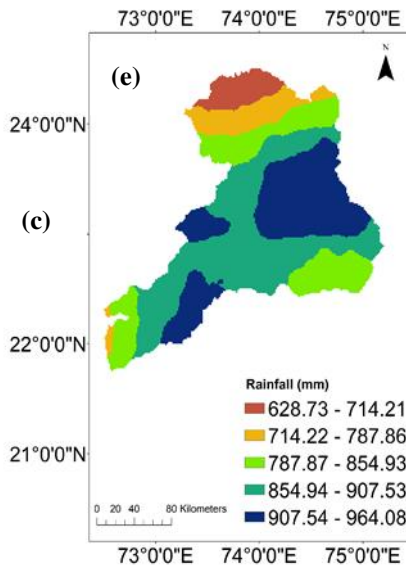
346



347

348

349

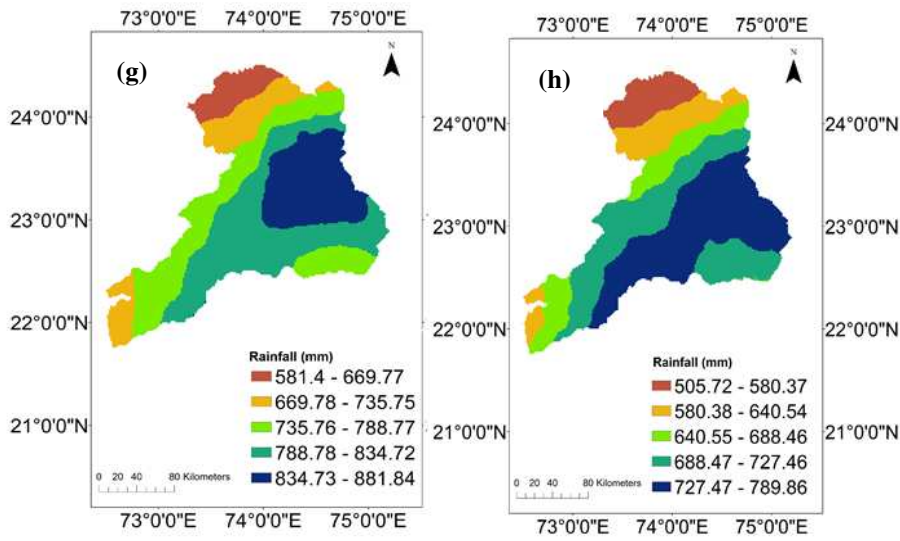


350

(e)

(f)

351



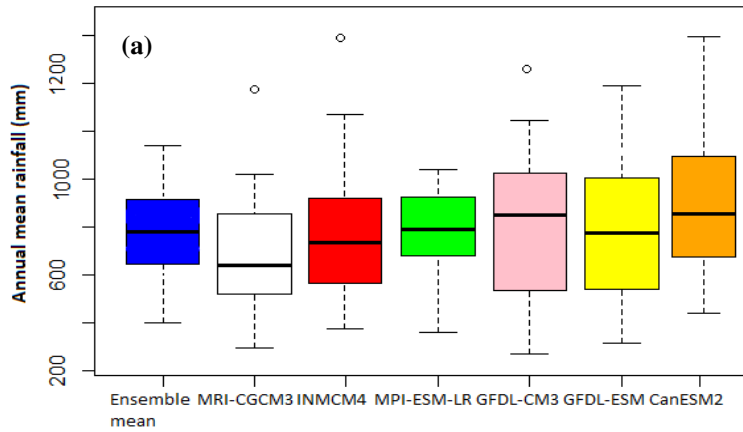
352

353

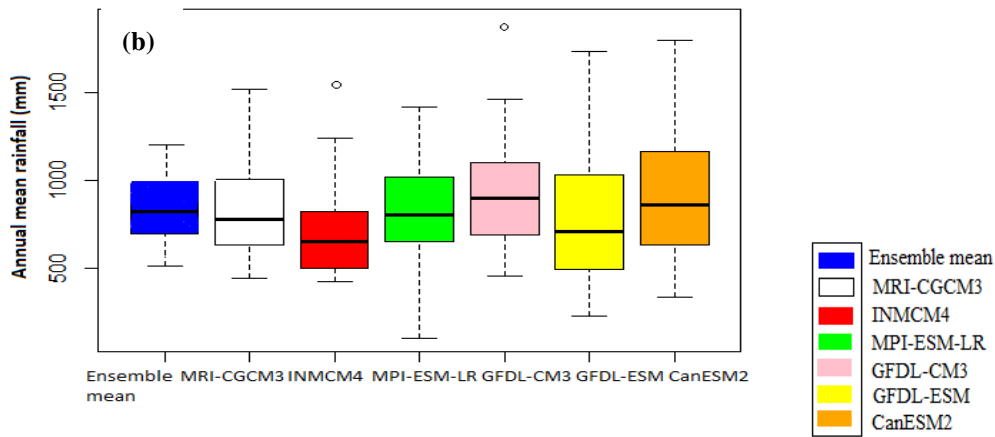
354 **Fig. 8 Spatial distribution of the annual mean rainfall during the time period**
355 **1981-2010: (a) IMD, (b) Ensemble mean, (c) MRI-CGCM3, (d) INMCM4, (e)**
356 **GFDL-CM3, (f) GFDL-ESM, (g) MPI-ESM-LR, (h) CanESM2.**

357

358 The box-whisker plots of the annual mean rainfall datasets for the period 1981-2010 and the
359 2011-2040 are shown in **Figure 9 (a-b)**. In the plot, boxes are having the upper quartile,
360 median line (center) and the lower quartile. The whiskers are represented as the dotted line at
361 each end of the box, and outliers are shown incircle. The annual mean rainfall of models has
362 median in the center which represents a uniform distribution of the rainfall.



363



364

365 **Fig.9 Box-Whisker plot of the annual mean rainfall datasets during the time periods (a)**
 366 **1981-2010 and (b) 2011-2040.**

367

368 **6.3 Input parameters of RUSLE**

369 The five major factors of RUSLE (R, K, LS, P and C) were estimated through the rainfall
 370 data, soil datasets, land use/land cover, DEM and satellite images as discussed in the
 371 following sections:

372

373 **6.3.1 Soil Erodibility Factor (K) and Topographic Factor (LS)**

374 The K factor varies from 0.034-0.052. The smaller value of K factor indicates lower
 375 permeability, low antecedent moisture content of soil and vice versa (Ganasri and Ramesh,

2016). The results indicated that the north part of the MRB showed the highest erodibility (0.052), and the central part and the north-east part show moderate to low erodibility (0.04-0.034) of the MRB as shown in **Figure 10(a)**.

The 0 value of LS is obtained in the south-west region of the MRB with the lowest elevation (1.79⁰ - 4.42⁰), while a value of 0.324 can be seen in the north-west part having the steepest slope (15.74⁰-50.59⁰) **Figure 10(b)**. The overall results suggested that the LS factor varies significantly between the north-west and the central part of the watershed.

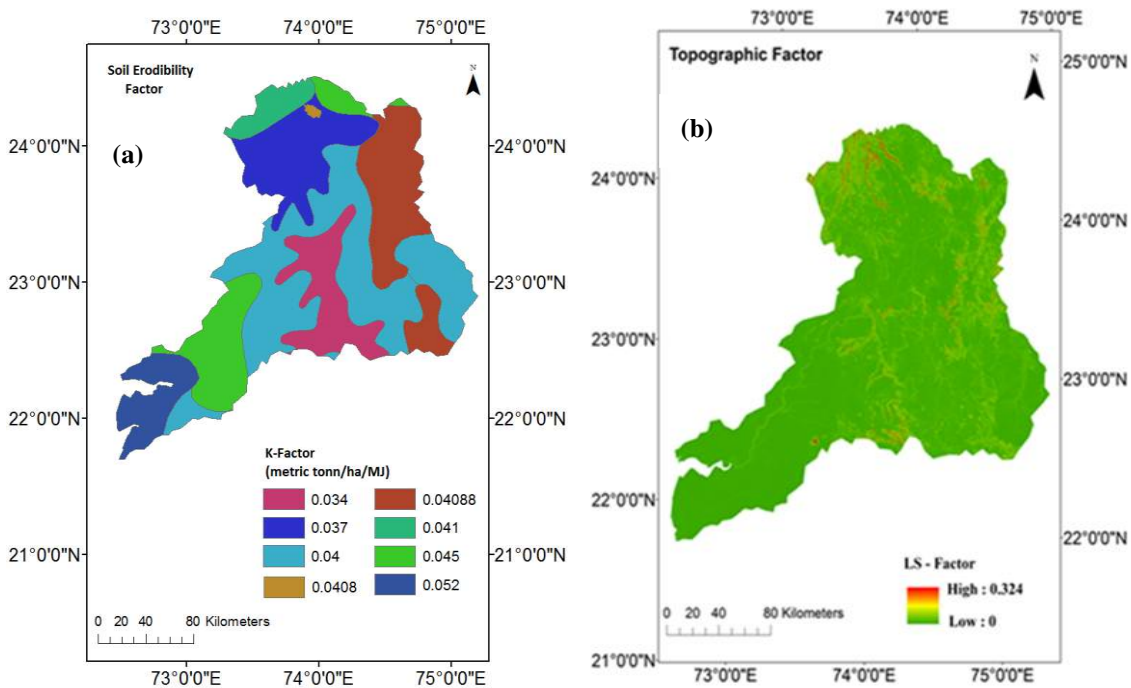


Fig.10 (a) Soil erodibility factor, (b) and Topographic factor of the study area

6.3.2 Crop Management Factor (C)

The value of C factor is assigned for particular land use class according to the literature survey (Rao, 1981a; Alexakis *et al.*, 2013). In general, the minimum value of C implies that the crop management practices are good and vice versa (Benkobi *et al.*, 1994; Biesemans *et al.*, 2000; Kouli *et al.*, 2009). The C factor of the base period 1981, 1991, 2001, 2011 and future 2040 land use/land cover are shown in **Figure 11**, while Table 4 illustrated the

391 percentages of the area occupied. On comparison with the baseline time period, finding
392 indicates that the C-factor of Urban, Barren, Cropland and Grassland area are increasing,
393 while for Water and Forest areas, a decreasing value is observed in 2040.

394

395 **Table 4. Percent land area for each C value calculated using the classified images of**
396 **different years.**

397

Classes	1981	1991	2001	2011	2040
Waterbody	6.50%	4.80%	4.50%	4.94%	4.06%
Forest	23.37%	45.00%	40.36%	25.66%	22.43%
Grassland	19.04%	7.40%	9.67%	6.11%	44.76%
Cropland	25.72%	28.17%	24.74%	48.00%	17.36%
Barren	22.34%	11.27%	15.67%	7.33%	11.65%
Urban	2.40%	3.00%	5.01%	3.19%	5.71%

398

399

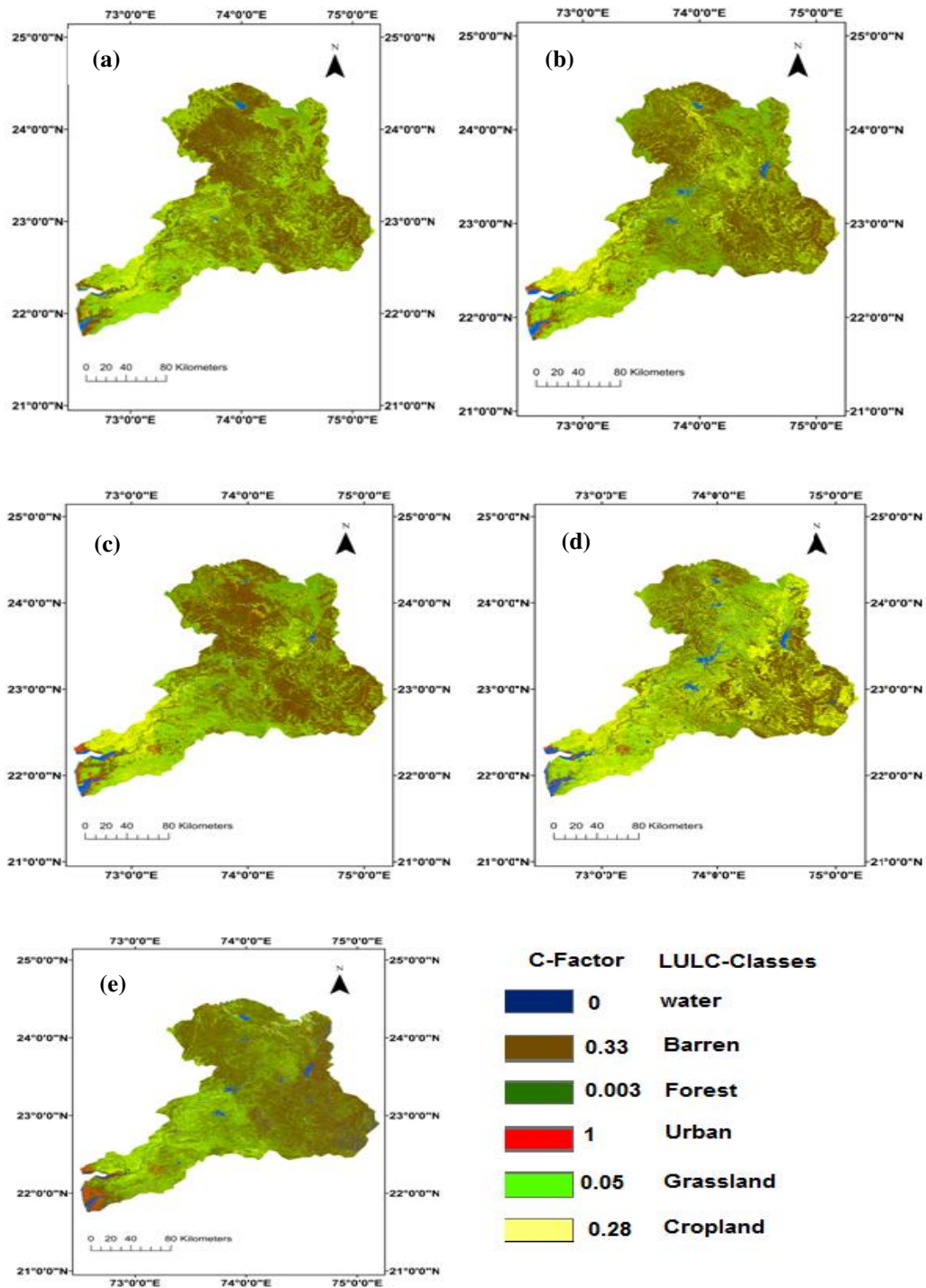
400

401

402

(a)

(b)



403

404 **Fig.11 C-factor of the study area in the year (a) 1981 (b) 1991 (c) 2001 (d) 2011 and (e)**

405 **2040**

406 **6.3.3 Conservation Practice Factor (P)**

407 In this study due to the absence of the field observation, the value of P factor is assigned
 408 on the basis of earlier studies (Mati *et al.*, 2000; Ganasri and Ramesh, 2016). The P-factor
 409 of the base period 1981, 1991, 2001, 2011 and future 2040 land use/land cover classes are
 410 shown in **Figure (12) and Table 5**, which illustrated the P-Factor percentage area occupied
 411 by different classes. On comparison with the base time period, the forest, grassland and
 412 cropland were found increasing while barren and water areas were decreased due to poor
 413 conservation practices.

414

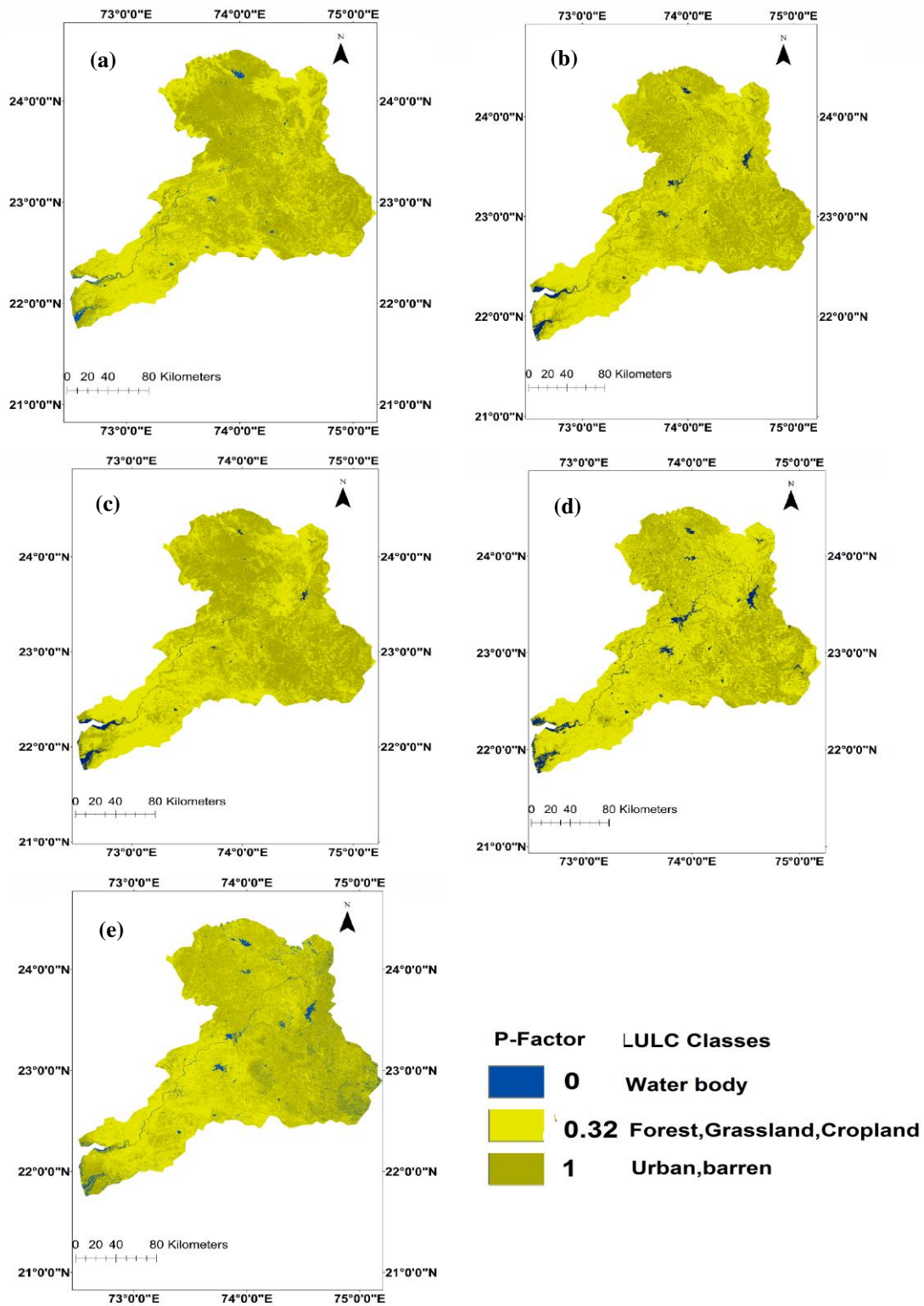
415 **Table 5. P-Factor calculated using the classified images of different years.**

Classes	1981	1991	2001	2011	2040
Water and Barren	29.84%	16.67%	20.20%	16.27%	23.71%
Cropland, Forest and Grassland	70.15%	80.91%	74.77%	80.78%	80.57%
Urban	2.40%	3.00%	5.01%	3.19%	5.71%

422

423

424



425

426 **Fig. 12 P-factor of the study area in the year (a) 1981, (b)1991, (c) 2001,(d) 2011, (e) and**

427 **2040**

428

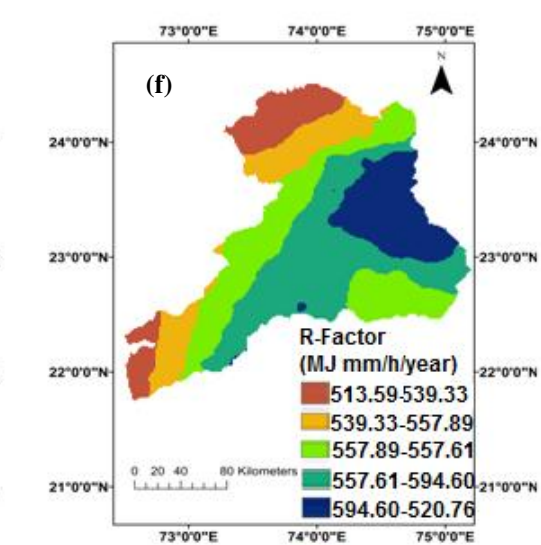
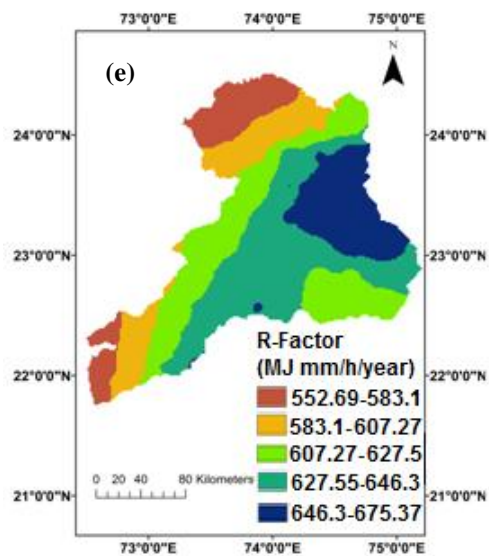
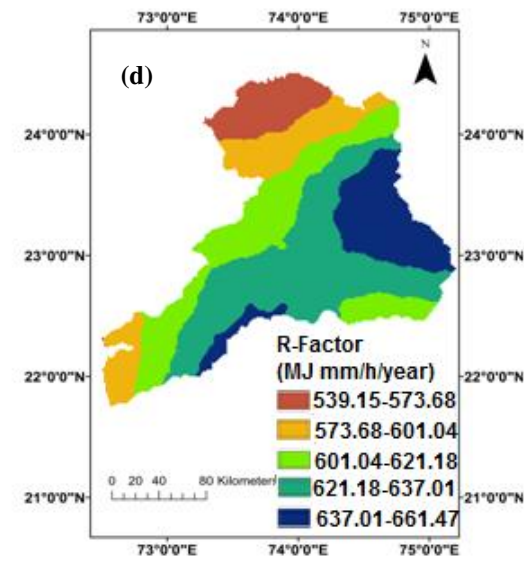
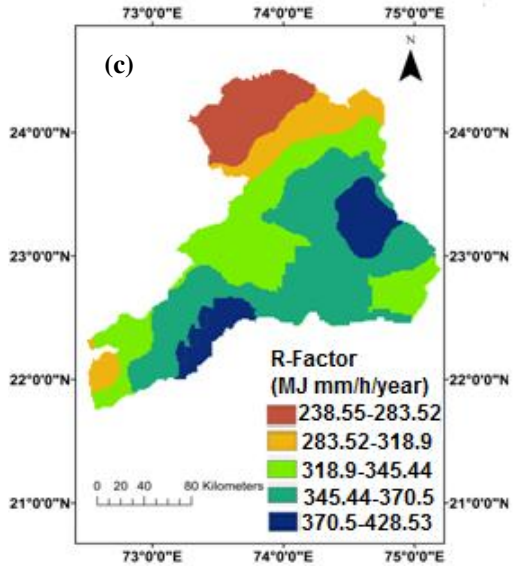
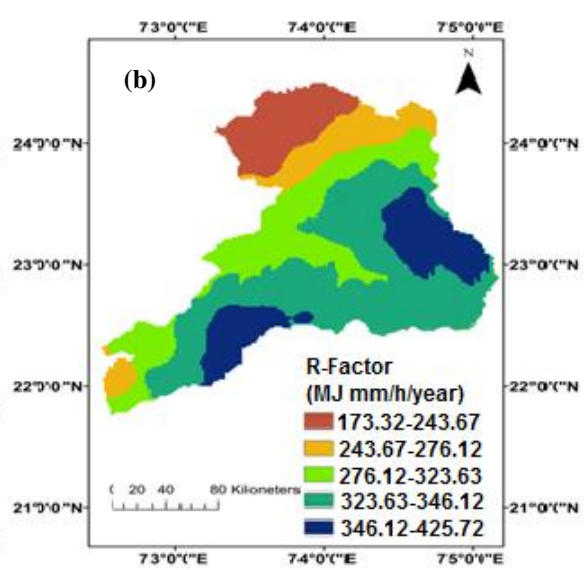
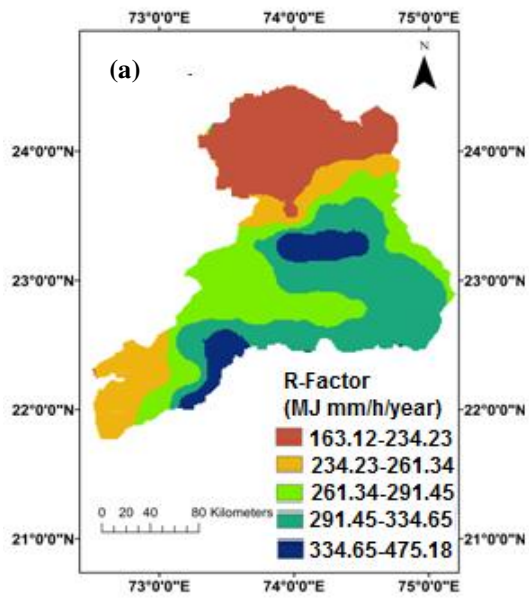
429 **6.3.4 Rainfall-Runoff Erosivity Factor (R)**

430 Many studies have suggested that the soil loss of a catchment is primarily affected by rainfall
431 (Pandey *et al.*, 2007; Nagaraju *et al.*, 2011b; Chatterjee *et al.*, 2014; Samanta and Bhunia,
432 2016). The mean annual rainfall-runoff erosivity of the base scenario (1981-1990),
433 (1991-2000), (2001-2010) and future scenario (2011-2040) are shown in **Figure (13)**. From
434 **Figure 13 (a)-(c)** the spatial distribution represents the highest erosivity in the north and the
435 north-west parts 290-450 MJ mm ha/h/y (1981-1990), 300-420 MJ mm ha/h/y (1991-2000),
436 345.45-426.53 MJ mm ha/h/y (2001-2010), the moderate value has been found in the central
437 part, and the lowest value observed in the east-south part 160-260 MJ mm ha/h/year
438 (1981-1990), 170-260 MJ mm ha/h/y (1991-2000), 238.55-318.9 MJ mm ha/h/y (2001-2010)
439 in the MRB.

440 However, during 2011-2040, the rainfall-runoff erosivity are estimated to be 675.16, 661.45
441 and 625.56 MJ mm ha/h/year for the MRI-CGCM3, the ensemble mean and the INMCM4
442 respectively, as shown in **Figure 13(e)-(f)**. By comparing with the base time period, it can be
443 seen that the rainfall-runoff erosivity increases gradually in the future scenario (2011-2040)
444 to approx. 36.88%, 35.57% and 31.88% in the MRI-CGCM3, the ensemble means and the
445 INMCM4 respectively.

446

447



449 **Fig.13 Rainfall-runoff erosivity during the time period (a) 1981-1990, (b) 1991-2000, (c)**
450 **2001-2010 of IMD, and (d-f) for the Ensemble mean, the MRI-CGCM3 and the**
451 **INMCM4 respectively, during the period 2011-2040.**

452

453 **6.4 The soil erosion assessment of the base scenario and validation**

454 Slope and terrain properties play a major role in shaping rate of soil erosion. Steep slopes are
455 prone to the more soil erosion as compared to the less steep slope. In the findings, the
456 north-west, the east and the central region of MRB are highly affected by the soil erosion
457 problem due to the steep slope and poor conservation practices along with intense rainfall.
458 However, the annual average soil loss was reported as 55.23 t/ha/y (1981-1990), 56.78 t/ha/y
459 (1991-2000), 57.35 t/ha/y (2000-2010) and categorized into five zones; very slight, slight,
460 moderate, moderate severe, and severe (see **Figure 14 (a)-(c)**).

461 South west portion of the MRB has coverage of very slight soil loss class zone. With each
462 passing decade the soil loss has increased by 1.55 t/ha/y and 0.57 t/ha/y. Increase in soil loss
463 could potentially occur due to the heavy rains and change in land use/land cover pattern. We
464 further explored the impact of land use and rainfall change impact on the soil erosion rate in
465 current and future scenarios. The National Bureau of Soil Survey and Land Use Planning
466 (NBSS & LUP)'s point based soil loss datasets (<http://www.bhoomigeoportal-nbsslup.in/>.)
467 are also in line with the obtained results. The datasets are categorized into very slight (<5
468 t/ha/y), slight (5-10 t/ha/y), moderate (10-15 t/ha/y), moderate severe (15-20 t/ha/y), severe
469 (20-40 t/ha/y), very severe classes (40-80 t/ha/y), and extremely severe classes (>80 t/ha/y)
470 are available from the site <http://www.bhoomigeoportal-nbsslup.in/>. The datasets showed a

471 similar soil loss values as obtained from the RUSLE model and the overall accuracy is found
472 as 85%. The category wise accuracy can be varied from very slight, slight, moderate to
473 severely eroded. Therefore, the result suggested that the RUSLE is a promising approach for
474 this type of the study as well as cost-effective in the identification of vulnerable area for soil
475 erosion risk.

476 **6.5 Soil erosion for the base and future scenarios**

477 Based on rainfall-runoff erosivity and land use change, soil erosion is predicted while other
478 factors influenced by the soil type and topography are kept constant while performing the
479 future projection. The changes in C-factor and P-factor along with R-factor increases
480 significantly in the future time series (2011-2040) in comparison to the present time series
481 (1981-2010). Similarly, the rate of the annual average soil erosion increases to 71.56, 66.34.
482 and 60.56 t/h/year in the MRI-CGCM3, the ensemble means and the INMCM4 model
483 respectively in future time series (2011-2040) **Figure 14 (d)-(f)**. As compared to the base
484 scenario, the annual average soil erosion increases to 29.56%, 20.11% and 11.21% in the
485 MRI-CGCM3, the INMCM4 and the ensemble mean model, respectively. As compared to
486 the soil erosion based on land use /land cover area, we find significant results, as the highest
487 soil erosion rate is recorded in forest class which is 217.13 to 327.45 t/ha/y and cropland
488 239.43 to 312.87 t/ha/y as shown in Table 6. The forest and cropland land cover area decrease
489 by 42.23% and 33.13% in the future scenario (2040), it may be the result of the expansion in
490 grassland and urban areas. Similarly, moderate soil erosion rates were found in the
491 grassland that is 110.63 to 128.96 t/ha/y along with a significant increase in land area of
492 approximately 47.34% due to the transition of forest and cropland areas and barren areas has

493 shown a soil erosion rates of 178.21 to 146.59 t/ha/y with an overall decrease in the land area
 494 of -1.23% due to the expansion of urban areas. While in urban area, the soil erosion rate was
 495 found to be the lowest 21.25 to 58.4 t/ha/y but the land area increased significantly to 72.32%
 496 from base to predicted future scenario. Projected increase in barren land and settlement area
 497 might affect the local rainfall mechanism in the basin but at the same time intense rainfall
 498 could exacerbates the rate and magnitude of land degradation by increased soil loss. With
 499 decrease in crop land and forest area in future scenario pose threat to natural ecosystem and
 500 biodiversity. Projected increase in a water body area is a good sign as far as future water
 501 demand and supply is concern in the MRB.

502 These results indicate that the change in soil erosion rate follows the rainfall and land use
 503 changes, which has been validated by various research articles, as Sharma *et al.*, suggested
 504 that mean soil erosion potential of the watershed was increased slightly due to the transition
 505 of LULC categories to cropland (Sharma *et al.*, 2011). Zare *et al.*, results indicate that mean
 506 soil erosion increases by 45% from the base period to future period, because of the most
 507 significant transition observed in the forest area to settlement (Zare *et al.*, 2017). Mondal and
 508 Gupta *et al.*, studies have reported that the increasing trend of precipitation and land use
 509 changes could increase the future rate of soil erosion over the Himalayan and Narmada River
 510 basin (Mondal *et al.*, 2016; Gupta and Kumar, 2017).

511 **Table.6 Average annual soil loss (t/ha/y) of different land use land covers classes.**

512

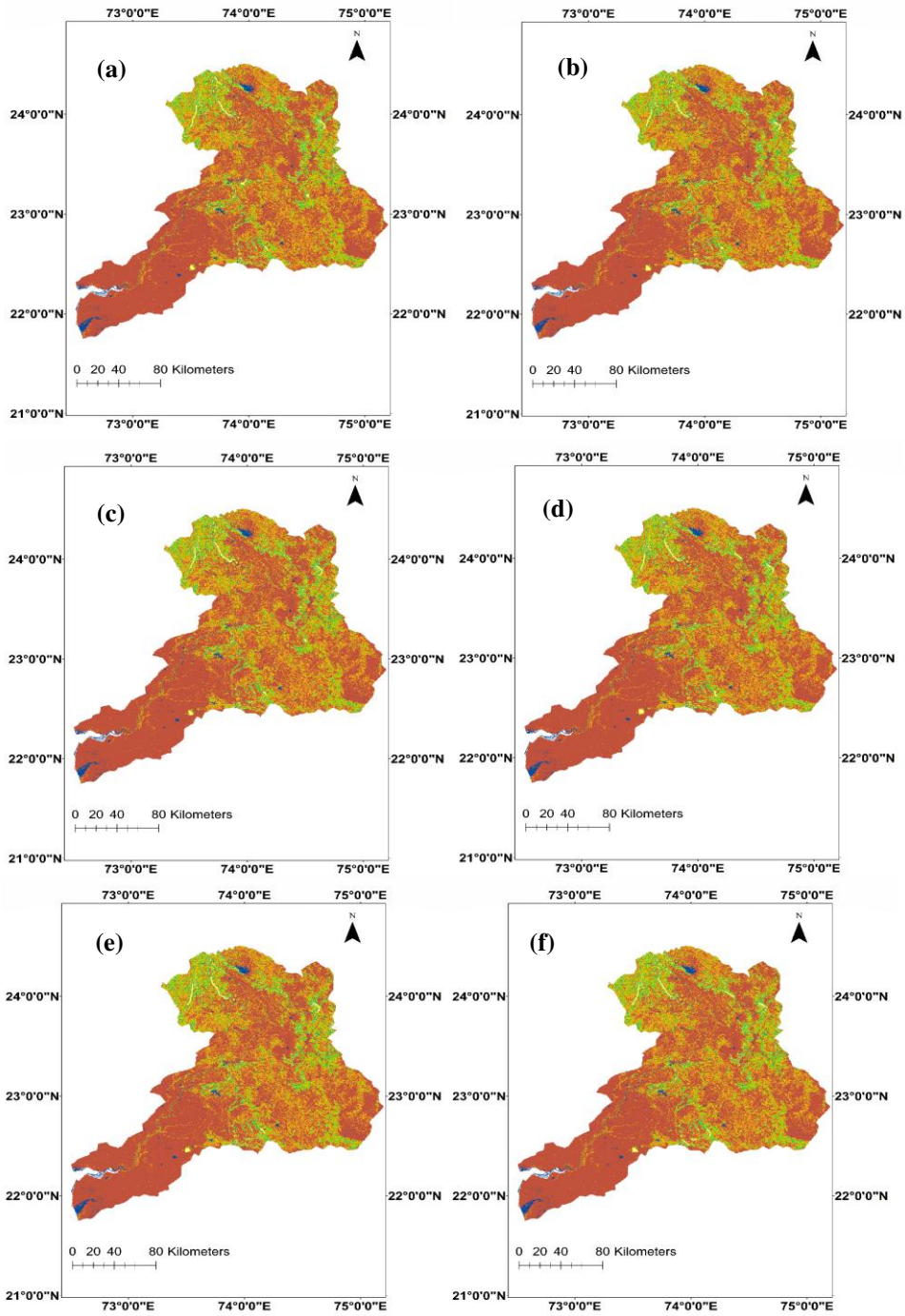
Classes	1981	1991	2001	2011	2040
---------	------	------	------	------	------

Forest	217.13	318.89	322.34	315.21	327.45
Grassland	110.63	117.32	125.25	131.89	128.96
Cropland	239.43	246.15	320.21	205.38	312.87
Barren	178.21	162.35	199.90	235.21	146.59
Urban	21.25	28.54	20.12	42.26	58.4

513

514

515



516

517 **Legend- soil loss (t/ha/y)**



518

519 **Fig.14. Soil erosion rate during the time period (a) 1981-1990 (b) 1991-2000 (c)**
520 **2001-2010 of IMD, and (d-f) for the Ensemble mean, the MRI-CGCM3 and the**
521 **INMCM4 respectively, during the time periods (2011-2040).**

522

523 **7. Conclusion**

524 The study demonstrated the potential impact of long-term rainfall and land use/land cover
525 changes on soil erosion using the state-of-the-art RUSLE and NEX-GDDP-CMIP5 models.

526 The results indicate that the RUSLE has potential to capture catchment characteristics
527 including climatic variables such as rainfall distribution, soil properties (texture, organic

528 carbon), topography (slope, flow accumulation), land use (crop pattern, management and
529 practices), and hence can help in the quantification of the soil erosion losses. The

530 MRI-CGCM3, INMCM4 and ensemble mean are the most suitable models to capture the
531 spatial variability of the precipitation with high spatial correlation (0.65-0.83) and low error

532 rate (0.52 mm/day) with respect to the observed (IMD) datasets, during the time period
533 1981-2010. The finding of land use changes during the time period 2040 reported that urban,

534 barren, cropland and grassland area with poor crop management practices are increasing
535 while water and forest area are decreasing. Furthermore, it is concluded that in near future the

536 rainfall erosivity factor may increase which can lead to high soil erosion rate. The outcome of
537 this study would be of important help in evaluating the landform and their processes,

538 agricultural productivity, hazardous mitigation and so forth within the study area and for
539 deducing the changes in the future. In addition, the results obtained from this study can be

540 utilized by various government agencies, developers and policymaker for a better soil and

541 water conservation in the MRB. Furthermore, the implementation of the proposed technique
542 is robust as it is based on satellite imagery and ancillary datasets provided globally at no cost.
543 The method is straight-forward, and requires low computational facility and hence can be
544 easily reapplied in other parts of the world to cover a broad spectrum of catchments.

545

546 **Acknowledgements**

547 The first author is highly thankful to the Department of Science and Technology,
548 Government of India for funding the research work. The authors would like to thank the
549 Banaras Hindu University for supporting this PhD research work and for providing necessary
550 funds.

551 **Conflicts of Interest:** The authors declare no conflict of interest.

552

553 **References**

- 554 Aburas, M.M., Ho, Y.M., Ramli, M.F., Ash'aari, Z.H., 2017. Improving the capability of an
555 integrated CA-Markov model to simulate spatio-temporal urban growth trends using an
556 Analytical Hierarchy Process and Frequency Ratio. *International Journal of Applied Earth
557 Observation and Geoinformation* 59, 65-78.
- 558 Alexakis, D.D., Hadjimitsis, D.G., Agapiou, A., 2013. Integrated use of remote sensing, GIS and
559 precipitation data for the assessment of soil erosion rate in the catchment area of "Yialias" in
560 Cyprus. *Atmospheric Research* 131, 108-124.
- 561 Angima, S., Stott, D., O'Neill, M., Ong, C., Weesies, G., 2003. Soil erosion prediction using
562 RUSLE for central Kenyan highland conditions. *Agriculture, ecosystems & environment* 97,
563 295-308.
- 564 Arnoldous, H., 1980. An approximation of the rainfall factor in the USLE in assessment of
565 Erosion. England: Wiley Chichester, 127-132.
- 566 Bao, Y., Wen, X., 2017. Projection of China's near-and long-term climate in a new
567 high-resolution daily downscaled dataset NEX-GDDP. *Journal of Meteorological Research* 31,
568 236-249.
- 569 Benkobi, L., Trlica, M., Smith, J.L., 1994. Evaluation of a refined surface cover subfactor for use
570 in RUSLE. *Rangeland Ecology & Management/Journal of Range Management Archives* 47,
571 74-78.

572 Biesemans, J., Van Meirvenne, M., Gabriels, D., 2000. Extending the RUSLE with the Monte
573 Carlo error propagation technique to predict long-term average off-site sediment
574 accumulation. *Journal of Soil and Water Conservation* 55, 35-42.

575 Bokhari, S.A.A., Ahmad, B., Ali, J., Ahmad, S., Mushtaq, H., Rasul, G., 2018. Future Climate
576 Change Projections of the Kabul River Basin Using a Multi-model Ensemble of High-Resolution
577 Statistically Downscaled Data. *Earth Systems and Environment* 2, 477-497.

578 Bonilla, C.A., Reyes, J.L., Magri, A., 2010. Water erosion prediction using the Revised Universal
579 Soil Loss Equation (RUSLE) in a GIS framework, central Chile. *Chilean Journal of Agricultural
580 Research* 70, 159-169.

581 Chatterjee, S., Krishna, A., Sharma, A., 2014. Geospatial assessment of soil erosion
582 vulnerability at watershed level in some sections of the Upper Subarnarekha river basin,
583 Jharkhand, India. *Environmental earth sciences* 71, 357-374.

584 Chaturvedi, R.K., Joshi, J., Jayaraman, M., Bala, G., Ravindranath, N., 2012. Multi-model
585 climate change projections for India under representative concentration pathways. *Current
586 Science* 103, 791-802.

587 Das, D., 2014. Identification of erosion prone areas by morphometric analysis using GIS.
588 *Journal of The Institution of Engineers (India): Series A* 95, 61-74.

589 Demirci, A., Karaburun, A., 2012. Estimation of soil erosion using RUSLE in a GIS framework: a
590 case study in the Buyukcekmece Lake watershed, northwest Turkey. *Environmental Earth
591 Sciences* 66, 903-913.

592 Duulatov, E., Chen, X., Amanambu, A.C., Ochege, F.U., Orozbaev, R., Issanova, G.,
593 Omurakunova, G., 2019. Projected Rainfall Erosivity Over Central Asia Based on CMIP5 Climate
594 Models. *Water* 11, 897.

595 Fernandez, C., Wu, J., McCool, D., Stöckle, C., 2003. Estimating water erosion and sediment
596 yield with GIS, RUSLE, and SEDD. *Journal of Soil and Water Conservation* 58, 128-136.

597 Fragou, S., Kalogeropoulos, K., Stathopoulos, N., Louka, P., Srivastava, P.K., Karpouzias, S., P
598 Kalivas, D., P Petropoulos, G., 2020. Quantifying Land Cover Changes in a Mediterranean
599 Environment Using Landsat TM and Support Vector Machines. *Forests* 11, 750.

600 Gajbhiye, S., Mishra, S., Pandey, A., 2014. Prioritizing erosion-prone area through
601 morphometric analysis: an RS and GIS perspective. *Applied Water Science* 4, 51-61.

602 Ganasri, B., Ramesh, H., 2016. Assessment of soil erosion by RUSLE model using remote
603 sensing and GIS-A case study of Nethravathi Basin. *Geoscience Frontiers* 7, 953-961.

604 Ghosh, P., Mukhopadhyay, A., Chanda, A., Mondal, P., Akhand, A., Mukherjee, S., Nayak, S.,
605 Ghosh, S., Mitra, D., Ghosh, T., 2017. Application of Cellular automata and Markov-chain
606 model in geospatial environmental modeling-A review. *Remote Sensing Applications: Society
607 and Environment* 5, 64-77.

608 Giorgi, F., Mearns, L.O., 2002. Calculation of average, uncertainty range, and reliability of
609 regional climate changes from AOGCM simulations via the "reliability ensemble
610 averaging"(REA) method. *Journal of Climate* 15, 1141-1158.

611 Gupta, S., Kumar, S., 2017. Simulating climate change impact on soil erosion using RUSLE
612 model- A case study in a watershed of mid-Himalayan landscape. *Journal of Earth System
613 Science* 126, 43.

614 Hagedorn, R., Doblas-Reyes, F.J., Palmer, T., 2005. The rationale behind the success of
615 multi-model ensembles in seasonal forecasting—I. Basic concept. *Tellus A: Dynamic*
616 *Meteorology and Oceanography* 57, 219-233.

617 Jain, S., Salunke, P., Mishra, S.K., Sahany, S., Choudhary, N., 2019. Advantage of NEX-GDDP
618 over CMIP5 and CORDEX Data: Indian Summer Monsoon. *Atmospheric Research*.

619 Jain, S.K., Kumar, V., 2012. Trend analysis of rainfall and temperature data for India. *Current*
620 *Science*, 37-49.

621 Karamesouti, M., Petropoulos, G.P., Papanikolaou, I.D., Kairis, O., Kosmas, K., 2016. Erosion
622 rate predictions from PESERA and RUSLE at a Mediterranean site before and after a wildfire:
623 Comparison & implications. *Geoderma* 261, 44-58.

624 Kliment, Z., Kadlec, J., Langhammer, J., 2008. Evaluation of suspended load changes using
625 AnnAGNPS and SWAT semi-empirical erosion models. *Catena* 73, 286-299.

626 Kouli, M., Soupios, P., Vallianatos, F., 2009. Soil erosion prediction using the revised universal
627 soil loss equation (RUSLE) in a GIS framework, Chania, Northwestern Crete, Greece.
628 *Environmental Geology* 57, 483-497.

629 Kumar, A., Devi, M., Deshmukh, B., 2014. Integrated remote sensing and geographic
630 information system based RUSLE modelling for estimation of soil loss in western Himalaya,
631 India. *Water resources management* 28, 3307-3317.

632 Liu, D., Tang, W., Liu, Y., Zhao, X., He, J., 2017. Optimal rural land use allocation in central
633 China: Linking the effect of spatiotemporal patterns and policy interventions. *Applied*
634 *Geography* 86, 165-182.

635 Markose, V.J., Jayappa, K., 2016. Soil loss estimation and prioritization of sub-watersheds of
636 Kali River basin, Karnataka, India, using RUSLE and GIS. *Environmental monitoring and*
637 *assessment* 188, 225.

638 Mati, B.M., Morgan, R.P., Gichuki, F.N., Quinton, J.N., Brewer, T.R., Liniger, H.P., 2000.
639 Assessment of erosion hazard with the USLE and GIS: A case study of the Upper Ewaso Ng'iro
640 North basin of Kenya. *International Journal of Applied Earth Observation and Geoinformation*
641 2, 78-86.

642 Maurer, E.P., Hidalgo, H.G., 2008. Utility of daily vs. monthly large-scale climate data: an
643 intercomparison of two statistical downscaling methods.

644 Mondal, A., Khare, D., Kundu, S., 2016. Impact assessment of climate change on future soil
645 erosion and SOC loss. *Natural Hazards* 82, 1515-1539.

646 Mondal, A., Khare, D., Kundu, S., Meena, P.K., Mishra, P., Shukla, R., 2014. Impact of climate
647 change on future soil erosion in different slope, land use, and soil-type conditions in a part of
648 the Narmada River Basin, India. *Journal of Hydrologic Engineering* 20, C5014003.

649 Montanarella, L., Badraoui, M., Chude, V., Costa, I., Mamo, T., Yemefack, M., AULANG, M.,
650 Yagi, K., Hong, S.Y., Vijarnsorn, P., 2015. Status of the world's soil resources: main report.
651 *Embrapa Solos-Livro científico (ALICE)*.

652 Moore, I.D., Wilson, J.P., 1992. Length-slope factors for the Revised Universal Soil Loss
653 Equation: Simplified method of estimation. *Journal of soil and water conservation* 47,
654 423-428.

655 Nagaraju, M., Reddy, G.O., Maji, A., Srivastava, R., Raja, P., Barthwal, A., 2011a. Soil loss
656 mapping for sustainable development and management of land resources in Warora Tehsil of

657 Chandrapur District of Maharashtra: An integrated approach using remote sensing and GIS.
658 Journal of the Indian society of remote sensing 39, 51-61.

659 Nagaraju, M.S., Obi Reddy, G., Maji, A., Srivastava, R., Raja, P., Barthwal, A., 2011b. Soil loss
660 mapping for sustainable development and management of land resources in Warora Tehsil of
661 Chandrapur District of Maharashtra: An integrated approach using remote sensing and GIS.
662 Journal of the Indian society of remote sensing 39, 51-61.

663 Nandi, I., Srivastava, P.K., Shah, K., 2017. Floodplain mapping through support vector machine
664 and optical/infrared images from Landsat 8 OLI/TIRS sensors: case study from Varanasi. Water
665 Resources Management 31, 1157-1171.

666 Naqvi, H.R., Mallick, J., Devi, L.M., Siddiqui, M.A., 2013. Multi-temporal annual soil loss risk
667 mapping employing revised universal soil loss equation (RUSLE) model in Nun Nadi
668 Watershed, Uttarakhand (India). Arabian journal of geosciences 6, 4045-4056.

669 Pai, D., Sridhar, L., Rajeevan, M., Sreejith, O., Satbhai, N., Mukhopadhyay, B., 2014.
670 Development of a new high spatial resolution (0.25× 0.25) long period (1901–2010) daily
671 gridded rainfall data set over India and its comparison with existing data sets over the region.
672 Mausam 65, 1-18.

673 Palmer, T., Doblas-Reyes, F., Hagedorn, R., Weisheimer, A., 2005. Probabilistic prediction of
674 climate using multi-model ensembles: from basics to applications. Philosophical Transactions
675 of the Royal Society B: Biological Sciences 360, 1991-1998.

676 Pan, J., Wen, Y., 2014. Estimation of soil erosion using RUSLE in Caijiamiao watershed, China.
677 Natural Hazards 71, 2187-2205.

678 Pandey, A., Chowdary, V., Mal, B., 2007. Identification of critical erosion prone areas in the
679 small agricultural watershed using USLE, GIS and remote sensing. Water resources
680 management 21, 729-746.

681 Pradeep, G., Krishnan, M.N., Vijith, H., 2015. Identification of critical soil erosion prone areas
682 and annual average soil loss in an upland agricultural watershed of Western Ghats, using
683 analytical hierarchy process (AHP) and RUSLE techniques. Arabian Journal of Geosciences 8,
684 3697-3711.

685 Pradhan, B., Chaudhari, A., Adinarayana, J., Buchroithner, M.F., 2012. Soil erosion assessment
686 and its correlation with landslide events using remote sensing data and GIS: a case study at
687 Penang Island, Malaysia. Environmental monitoring and assessment 184, 715-727.

688 Prasannakumar, V., Vijith, H., Abinod, S., Geetha, N., 2012. Estimation of soil erosion risk
689 within a small mountainous sub-watershed in Kerala, India, using Revised Universal Soil Loss
690 Equation (RUSLE) and geo-information technology. Geoscience Frontiers 3, 209-215.

691 Rajeevan, M., Nayak, S., 2017. Observed climate variability and change over the Indian region.
692 Springer.

693 Rao, Y., 1981a. Evaluation of cropping management factor in universal soil loss equation under
694 natural rainfall condition of Kharagpur, India. Proceedings of Southeast Asian regional
695 symposium on problems of soil erosion and sedimentation, 1981. Asian Institute of
696 Technology, pp. 241-254.

697 Rao, Y., 1981b. Evaluation of cropping management factor in Universal Soil Loss Equation
698 under natural rainfall conditions of Kharagpur, India. Proceedings of the South-East Asian
699 Regional Symposium on Problems of Soil Erosion and Sedimentation, held at Asian Institute of

700 Technology, January 27-29, 1981/edited by T. Tingsanchali, H. Eggers. Bangkok, Thailand: The
701 Institute, 1981.

702 Renard, K.G., 1997. Predicting soil erosion by water: a guide to conservation planning with the
703 revised universal soil loss equation (RUSLE).

704 Renard, K.G., Foster, G.R., Weesies, G., McCool, D., Yoder, D., 1997. Predicting soil erosion by
705 water: a guide to conservation planning with the Revised Universal Soil Loss Equation (RUSLE).
706 United States Department of Agriculture Washington, DC.

707 Renard, K.G., Foster, G.R., Weesies, G.A., Porter, J.P., 1991. RUSLE: Revised universal soil loss
708 equation. *Journal of soil and Water Conservation* 46, 30-33.

709 Renschler, C., Diekkrüger, B., Mannaerts, C., 1999. Regionalization in surface runoff and soil
710 erosion risk evaluation. IAHS Publication(International Association of Hydrological Sciences),
711 233-241.

712 Sahany, S., Mishra, S.K., Salunke, P., 2019. Historical simulations and climate change
713 projections over India by NCAR CCSM4: CMIP5 vs. NEX-GDDP. *Theoretical and Applied*
714 *Climatology* 135, 1423-1433.

715 Samanta, R.K., Bhunia, G.S., 2016. Spatial modelling of soil erosion susceptibility mapping in
716 lower basin of Subarnarekha river (India) based on geospatial techniques. *Modeling Earth*
717 *Systems and Environment* 2, 1-13.

718 Sharma, A., Tiwari, K.N., Bhadoria, P., 2011. Effect of land use land cover change on soil
719 erosion potential in an agricultural watershed. *Environmental monitoring and assessment* 173,
720 789-801.

721 Sharpley, A., Williams, J., 1990. EPIC-erosion/productivity impact calculator: 1. Model
722 documentation.

723 Singh, S.K., Srivastava, P.K., Gupta, M., Thakur, J.K., Mukherjee, S., 2014. Appraisal of land
724 use/land cover of mangrove forest ecosystem using support vector machine. *Environmental*
725 *earth sciences* 71, 2245-2255.

726 Srivastava, P.K., Han, D., Rico-Ramirez, M.A., Bray, M., Islam, T., 2012. Selection of
727 classification techniques for land use/land cover change investigation. *Advances in Space*
728 *Research* 50, 1250-1265.

729 Stefanidis, S., Stathis, D., 2018. Effect of Climate Change on Soil Erosion in a Mountainous
730 Mediterranean Catchment (Central Pindus, Greece). *Water* 10, 1469.

731 Taylor, K.E., 2001. Summarizing multiple aspects of model performance in a single diagram.
732 *Journal of Geophysical Research: Atmospheres* 106, 7183-7192.

733 Teng, H., Liang, Z., Chen, S., Liu, Y., Rossel, R.A.V., Chappell, A., Yu, W., Shi, Z., 2018. Current
734 and future assessments of soil erosion by water on the Tibetan Plateau based on RUSLE and
735 CMIP5 climate models. *Science of the Total Environment* 635, 673-686.

736 Thomas, J., Joseph, S., Thrivikramji, K., 2018. Assessment of soil erosion in a tropical mountain
737 river basin of the southern Western Ghats, India using RUSLE and GIS. *Geoscience Frontiers* 9,
738 893-906.

739 Tirkey, A.S., Pandey, A., Nathawat, M., 2013. Use of satellite data, GIS and RUSLE for
740 estimation of average annual soil loss in Daltonganj watershed of Jharkhand (India). *Journal of*
741 *Remote Sensing Technology* 1, 20-30.

742 Weng, Q., 2002. Land use change analysis in the Zhujiang Delta of China using satellite remote
743 sensing, GIS and stochastic modelling. *Journal of environmental management* 64, 273-284.

744 Wischmeier, W.H., Smith, D.D., 1978. Predicting rainfall erosion losses-a guide to conservation
745 planning. Predicting rainfall erosion losses-a guide to conservation planning.
746 Wood, A.W., Leung, L.R., Sridhar, V., Lettenmaier, D., 2004. Hydrologic implications of
747 dynamical and statistical approaches to downscaling climate model outputs. Climatic change
748 62, 189-216.
749 Yue-Qing, X., Xiao-Mei, S., Xiang-Bin, K., Jian, P., Yun-Long, C., 2008. Adapting the RUSLE and
750 GIS to model soil erosion risk in a mountains karst watershed, Guizhou Province, China.
751 Environmental monitoring and assessment 141, 275-286.
752 Yulianto, F., Maulana, T., Khomarudin, M.R., 2018. Analysis of the dynamics of land use change
753 and its prediction based on the integration of remotely sensed data and CA-Markov model, in
754 the upstream Citarum Watershed, West Java, Indonesia. International Journal of Digital Earth.
755 Zare, M., Panagopoulos, T., Loures, L., 2017. Simulating the impacts of future land use change
756 on soil erosion in the Kasilian watershed, Iran. Land Use Policy 67, 558-572.

757